CHAPTER 3 EXPERIMENTAL INVESTIGATIONS

This chapter describes the experimental tests, testing machines, and equipment used in this study. The experimental investigations were divided into three main parts, concerning materials, formability characterization and experimental procedure for constructing the damage curves. First, experiments were performed to determine all basic material properties of the investigated AHS steels, namely, Dual Phase (DP), TRansformation Induced Plasticity (TRIP) and galvannealed multiphase steel grade JAC780Y. Secondly, formability of these steels was characterized. Lastly, experiments for identifying damage initiation and generating damage curves were carried out for the JAC780Y steel sheet.

3.1 Materials characterization

The commercial advanced high strength (AHS) steel sheets DP780, TRIP780 with a thickness of 1.2 mm and JAC780Y with a thickness of 1.0 mm were investigated to find the materials characterization. The micrographs of both steels were illustrated in Figure 3.1. The microstructure of the DP steel mainly consisted of martensitic islands embedded in a ferritic matrix, as depict in Figure 3.1(a). The TRIP steel exhibit the microstructure containing ferritic matrix, bainite, retained austenite and small fraction of martensitic islands, as demonstrate in Figure 3.1(b).The multi-phase steel grade JAC780Y exhibited the same microstructure with DP steel and increasing metallurgical process as illustrate in Figure 3.1(c). The phase transformation from the austenitic phase to martensite occurs when TRIP steel is subjected to a sufficient deformation by mechanical loading [53,54]. The formation of martensite increases the rate of work hardening, which, in turn, raises the ductility of the material. This typical TRIP effect causes the TRIP steel to generally exhibit higher elongation than the DP steel at a comparable tensile strength [55,56]. Note that, in this work the TRIP effect was incorporated in the FE simulations by experimentally obtained flow curves. The transformation itself occurred in the formed samples was not modelled. However, its effect was fully accounted for in the determined stress-strain curve. Various mechanical tests were conducted in order to characterize the stress-strain and yield behaviors and to determine the material parameters for the applied hardening models under different states of deformation.

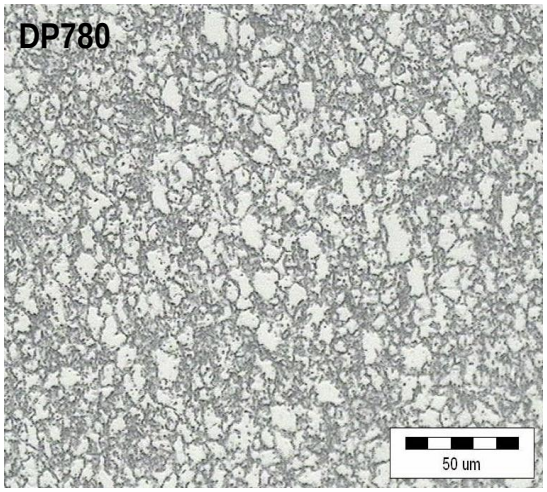

(a)

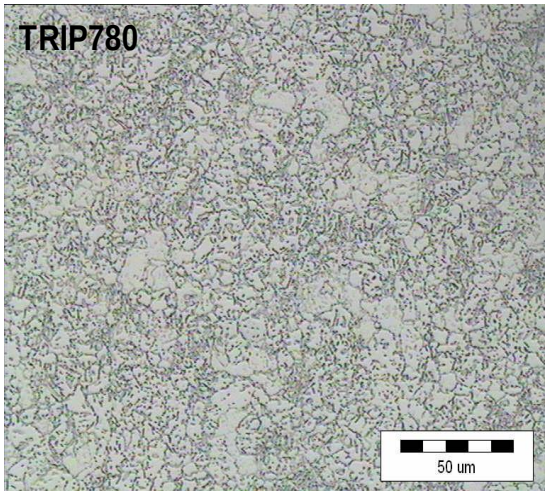

(b)

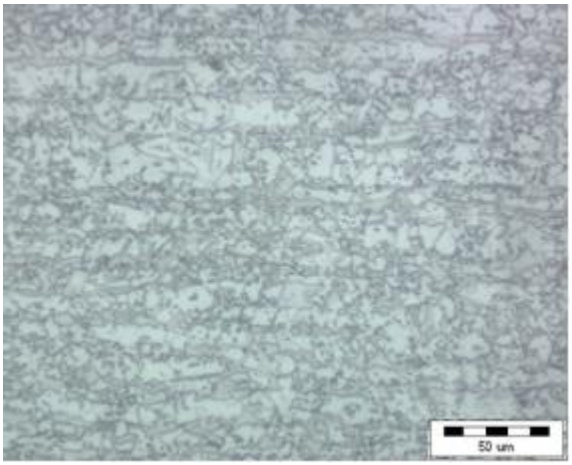

(c)

Figure 3.1 Microstructure of the investigated (a) DP780 (b) TRIP780 (c) JAC780Y steels.

Simple uniaxial tension tests have been widely used to determine material parameters for yield function and hardening models when characterizing the constitutive behavior of a material. However, for more complicated constitutive models, experimental data from other tests have been also developed. For example, the hydraulic bulge test and the disk compression test were proposed to determine the unknown parameters in the Yld2000-2d criterion. The objective of the present study is to evaluate various constitutive models with different characterization approaches. First, for the yield criterion, three yield functions are to be used (1) von Mises isotropic yield function, (2) Hill's 1948 anisotropic model, and (3) Yld2000-2d non-quadratic anisotropic model. Even for the same yield function, the material parameters can be obtained from different experimental approaches. For example, the parameters of Hill's 1948 model can refer to the yield stress or r-value in three different material orientations. Similarly, the reference flow hardening curve can be provided by any proportional test such as uniaxial tension, balanced biaxial tension. Therefore, in the following sections, several important mechanical tests for the characterization of basic mechanical properties are introduced.

3.1.1 Uniaxial tensile test

Uniaxial tensile tests were performed on a universal MTS testing machine at Materials Mechanics Laboratory, Graduate Institute of Ferrous Technology, Pohang University of Science and Technology (MML, GIFT, POSTECH). The testing machine is shown in Figure 3.2, by using the ASTM E8 standard specimen as illustrated in Figure 3.3. The samples prepared along three directions 0°, 45° and 90° from the rolling direction (RD) were investigated. Two mechanical extensometers were attached to the specimens during the tests for measuring longitudinal elongation and width reduction within the gauge length area. The crosshead speed of the machine was adjusted to ensure a strain rate of 0.001 s^{-1} for all tests. The yield strength (YS), ultimate tensile strength (UTS), uniform elongation, total elongation and *r*-value for each loading direction were obtained for investigating AHS steels grade DP780, TRIP780 and JAC780Y as demonstrated in Table 3.1 - Table 3.3, respectively. The obtained yield stresses were normalized by the uniaxial yield stress of the rolling direction. The *r*-values were calculated by linear approximations of the true width and true thickness strains measured up to the elongation of 14%. The normalized yield stresses and *r*-values of the

investigated steel for different directions were presented together in Table 3.4 to Table 3.6. The determined plastic true stress-strain curves from different directions were compared for TRIP780 steel sheet in Figure 3.4 and also JAC780Y in Figure 3.5. The DP steel exhibited somewhat higher yield strengths and ultimate strengths, but lower uniform and total elongation. This could be due to the martensitic transformation occurred during deformation of the TRIP780 steel. The *r*-values of the DP and TRIP steels were close to 1 in all directions. Nevertheless, the *r*-values of the DP steel were a bit smaller than those of the TRIP steel that was corresponding to the forming abilities of both steels.

Figure 3.2 MTS Universal Testing Machine

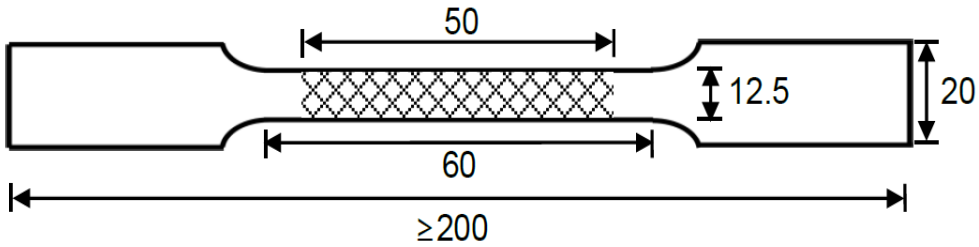

Figure 3.3 Schematic of the ASTM E8 tensile test specimen [57]

Table 3.1 Uniaxial tension properties for the DP780 steel (engineering value)

Direction (degree)	YS (MPa)	UTS (MPa)	%Elongation		r-value
			Uniform	Total	
0º	556.86	860.04	12.81	19.89	0.802
45º	525.11	845.29	15.35	20.92	0.849
90º	511.37	854.95	14.19	18.66	0.960

Table 3.2 Uniaxial tension properties for the TRIP780 steel (engineering value)

Direction (degree)	YS (MPa)	UTS (MPa)	%Elongation		r-value
			Uniform	Total	
0º	508.44	837.01	16.91	23.92	0.881
45º	525.39	842.14	17.82	24.03	1.002
90º	537.34	850.19	17.06	22.46	1.197

Table 3.3 Uniaxial tension properties for the JAC780Y (engineering value)

Direction (degree)	YS (MPa)	UTS (MPa)	%Elongation		r-value
			Uniform	Total	
0º	526.31	812.97	12.00	21.36	0.7986
45º	550.29	816.63	13.14	20.97	0.9756
90º	556.86	820.12	11.30	18.64	0.8571

Table 3.4 Normalized flow stresses and *r*-values for the DP780 steel

DP780	0°	45°	90°	Balanced biaxial
Normalized flow stress	1.0000	0.9556	0.9166	1.0469
r-value	0.802	0.849	0.960	0.926

Table 3.5 Normalized flow stresses and *r*-values for the TRIP780 steel

TRIP780	0°	45°	90°	Balanced biaxial
Normalized flow stress	1.0000	1.0244	1.0561	1.0889
r-value	0.881	1.002	1.197	0.900

Table 3.6 Normalized flow stresses and *r*-values for the JAC780Y steel.

JAC780Y	0°	45°	90°	Balanced biaxial
Normalized flow stress	1.0000	1.0270	1.0500	1.3260
r-value	0.7986	0.9756	0.8571	1.0220

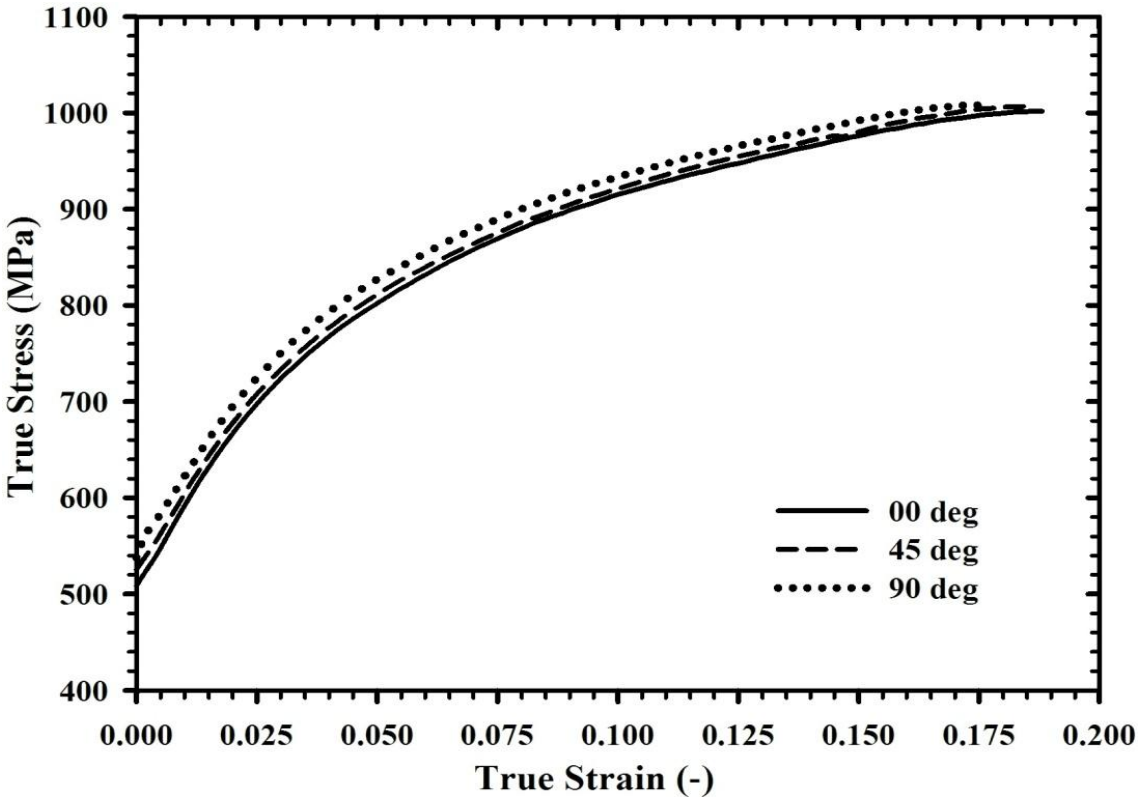

Figure 3.4 True stress-true strain curves from different testing directions determined by uniaxial tensile tests of the investigated TRIP780 steel.

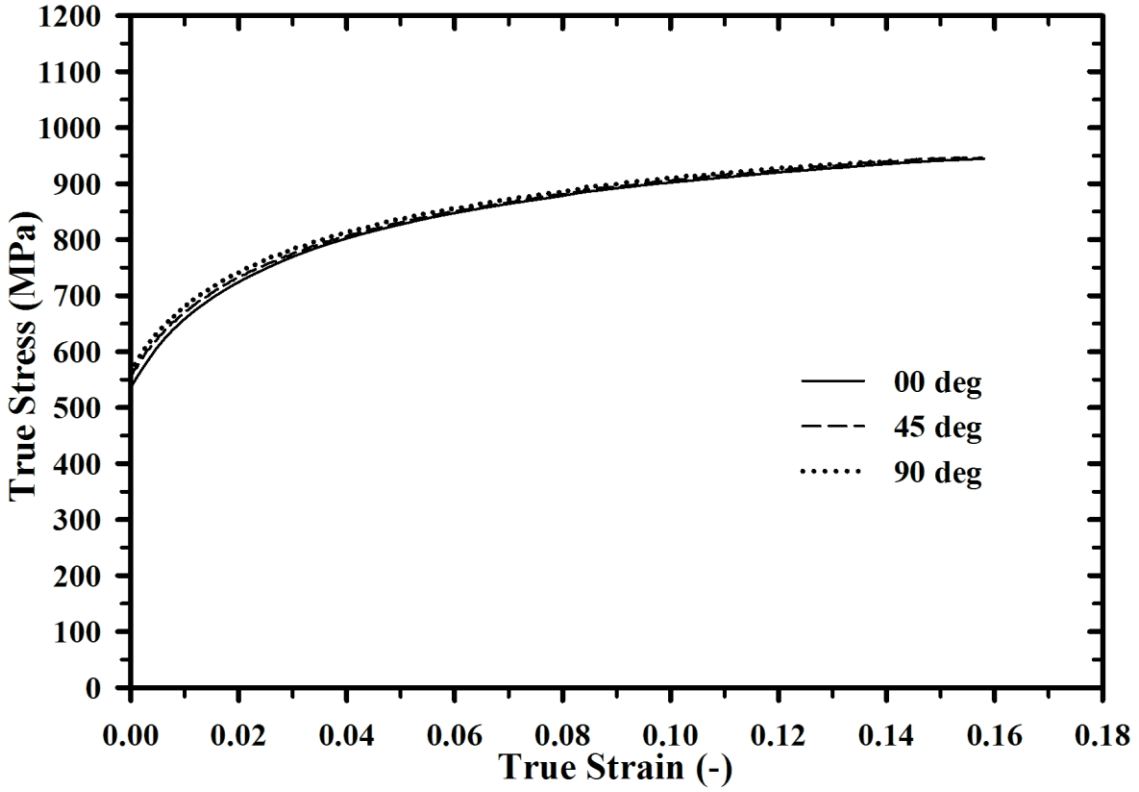

Figure 3.5 True stress-true strain curves from different testing directions determined by uniaxial tensile tests of the investigated JAC780Y steel

3.1.2 Hydraulic bulge test

As explained in the previous chapter, for advanced yield functions Yld2000-2d, the identification of anisotropy coefficients requires data in the balanced biaxial tension. Moreover, the balanced biaxial tension tests can provide reliable strain hardening curve to higher strain than uniaxial tension test. The biaxial stress-strain curve obtained from the hydraulic bulge test, which is usually more suitable to represent state of stress in most sheet forming processes. In order to characterize the strain hardening behavior in balanced biaxial tension stress state, a hydraulic bulge tester equipped with a mechanical measurement system was installed in this work, and the stress-strain curve obtained from this system was analyzed in terms of the data reproducibility, accuracy.

Hydraulic bulge tests were conducted on the Erichsen bulge/FLC tester model 161, in which has been belonged to MML-GIFT-POSTECH as illustrated in Figure 3.6. Generally, the bulge test has been successfully applied for investigating the biaxial flow behaviour of material. The experimental procedure and tool geometry can be found in [58] for details. A schematic view of the test is shown in Figure 3.7. During the test, the square specimen with a size of 300×300 mm^2 (Figure 3.8) was first clamped between the lower blank holder and the upper die. For AHS steel with ultimate tensile strength 780 MPa, the draw-in of the outer sample periphery was prevented by a drawbead and a high constant blank holding force of 1000 kN. Then, the velocity of the punch, which built up a hydraulic pressure against the specimens, was set to 12 mm/min to deform the specimen. When a predefined drawing force was reached or the specimen fractured, the pressure was released, and then the blank holder moved downwards to free the specimen. It was found that this velocity resulted in a thickness strain rate of about 0.003 s^{-1}. The oil pressure was recorded by a pressure sensor installed in the machine. A mechanical strain measurement device, as illustrated in Figure 3.9, was placed on the top surface of the specimen. It included an extensometer, a tripod and a Linear Variable Differential Transformer (LVDT). The in-plane displacement L was measured by the extensometer and the height difference h between the center and tripod on the sample curvature was obtained by the LVDT [13].In the hydraulic bulge tests, stress-strain relationship could be generally described by von Mises effective stress and strain, which corresponded to the balanced biaxial stress and thickness strain at the pole. According to the membrane theory, the balanced biaxial stress or membrane stress could be given as

$$\sigma_b = \frac{pR}{2t} \tag{3.1}$$

Where p is the bulge pressure and R indicates the radius of curvature at the pole, defined as $R = \left(a^2 + h^2\right)/2h$. The thickness t could be calculated through the relationship $t = t_0 \exp\left(-\varepsilon_t\right)$, in which t_0 was the initial thickness. The thickness strain ε_t was then obtained by [58]

$$\varepsilon_t = 2\ln\left(\frac{2R\sin^{-1}\left(L/2R\right)}{L_0}\right) \tag{3.2}$$

The in-plane displacement L was measured along 45° from the rolling direction of the sheet in these tests.

Figure 3.6 Erichsen bulge/FLC tester tester model 161

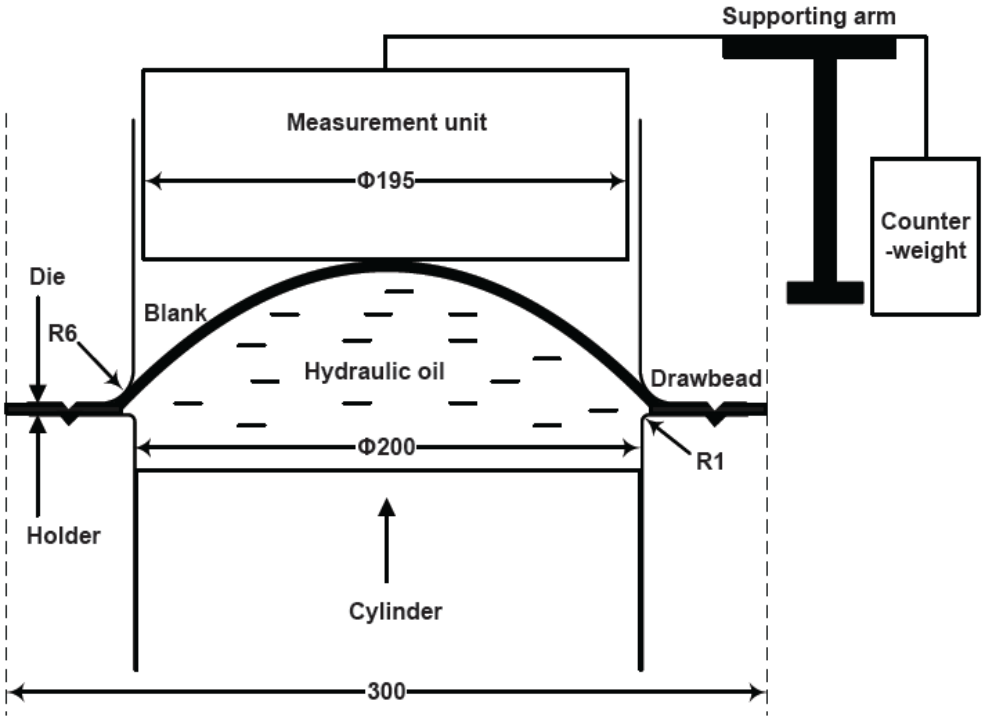

Figure 3.7 Schematic view of Erichsen bulge/FLC tester model 161[13]

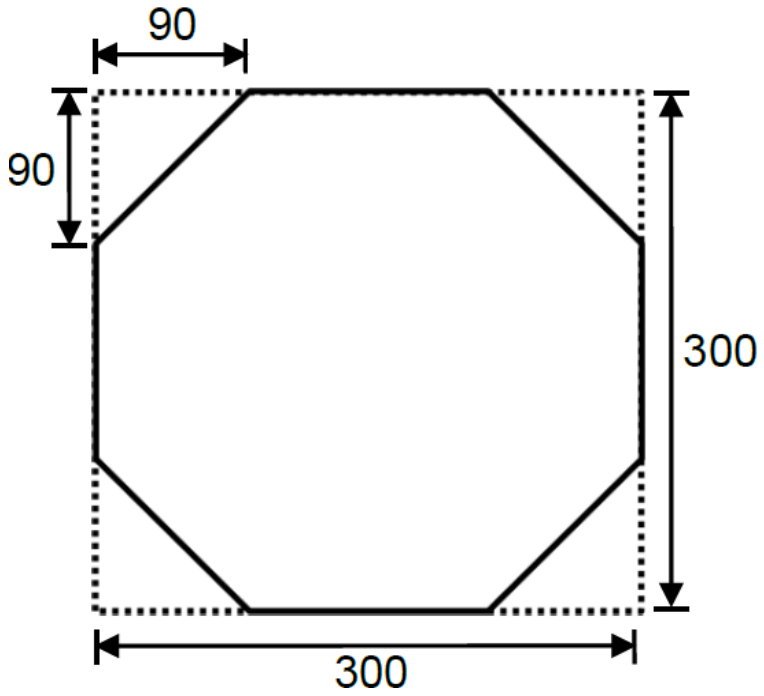

Figure 3.8 Specimen geometry for hydraulic bulge test [57]

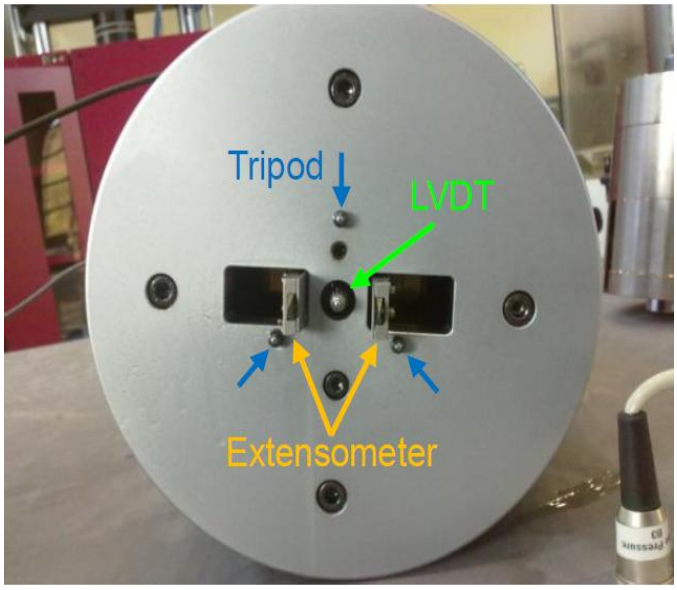

(a)

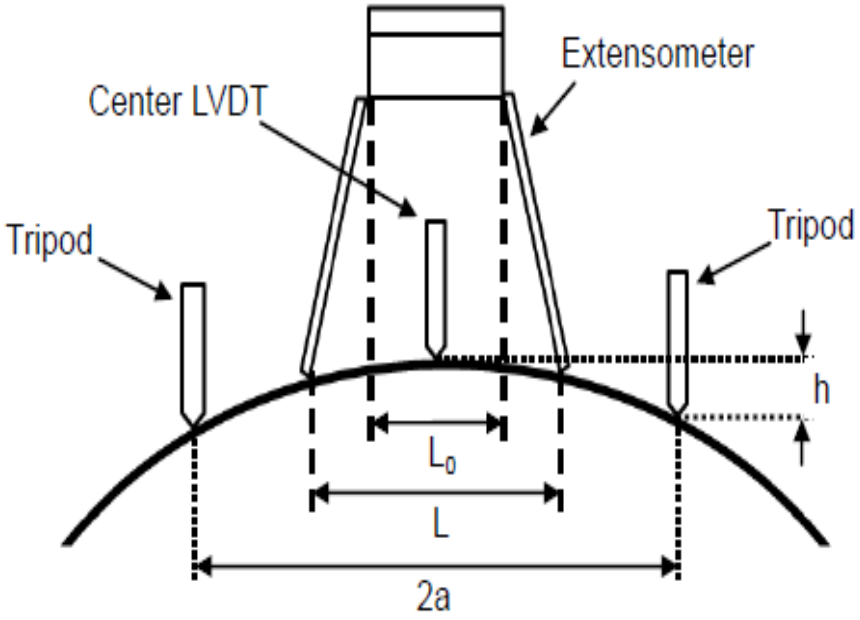

(b)

Fig. 3.9 (a) Mechanical measurement device for bulge test
(b) Schematic of the mechanical strain measurement device [57]

Demonstratively, the true stress-strain curve of the investigated steel grade TRIP780 determined by the bulge test was compared with that from the uniaxial tensile test in Figure 3.10. Both stress-strain curves were comparable, whereas the biaxial stress-strain curve exhibited higher strain and slightly higher strain hardening rate. The stress-strain response obtained from the hydraulic bulge test is usually more suitable for representing state of stress in most sheet metal forming processes. The yield stress under balanced biaxial tension (σ_b) was calculated based on the work-equivalence principle by compromising the biaxial and uniaxial tension flow curves. The averaged value of flow stress ratio σ_b/σ_0 was given in Table 3.5 as well. Note that no TRIP effect was considered in the FE modeling. It was presumed that the TRIP effect mechanism has been already taken into account by the applied flow curve. In the same manner, the stress-strain curves of the DP780 and JAC780Y steels were experimentally determined by hydraulic bulge test and tensile test in comparison and will be illustrated in Figure 3.16 and Figure 3.17, respectively.

3.1.3 Disk compression test

Through thickness disk compression tests were conducted for determining materials plastic anisotropy under the balanced biaxial tension state of stress. As shown in Figure 3.11, the compression platen was installed in MTS testing machine, was performed at MML-GIFT-POSTECH. Procedure of the disk compression test was described elsewhere in details [7, 59].The DP780 and TRIP780 sheet samples with a thickness of 1.2 mm and JAC780Y sheet samples with a thickness of 1.0 mm were upset through the sheet normal direction (ND).These specimens were cutting by wire cutting process with a diameter of 6 mm as depicted in Figure 3.12. To minimize the effects of friction, grease plus graphite was uniformly applied on the sample surfaces.

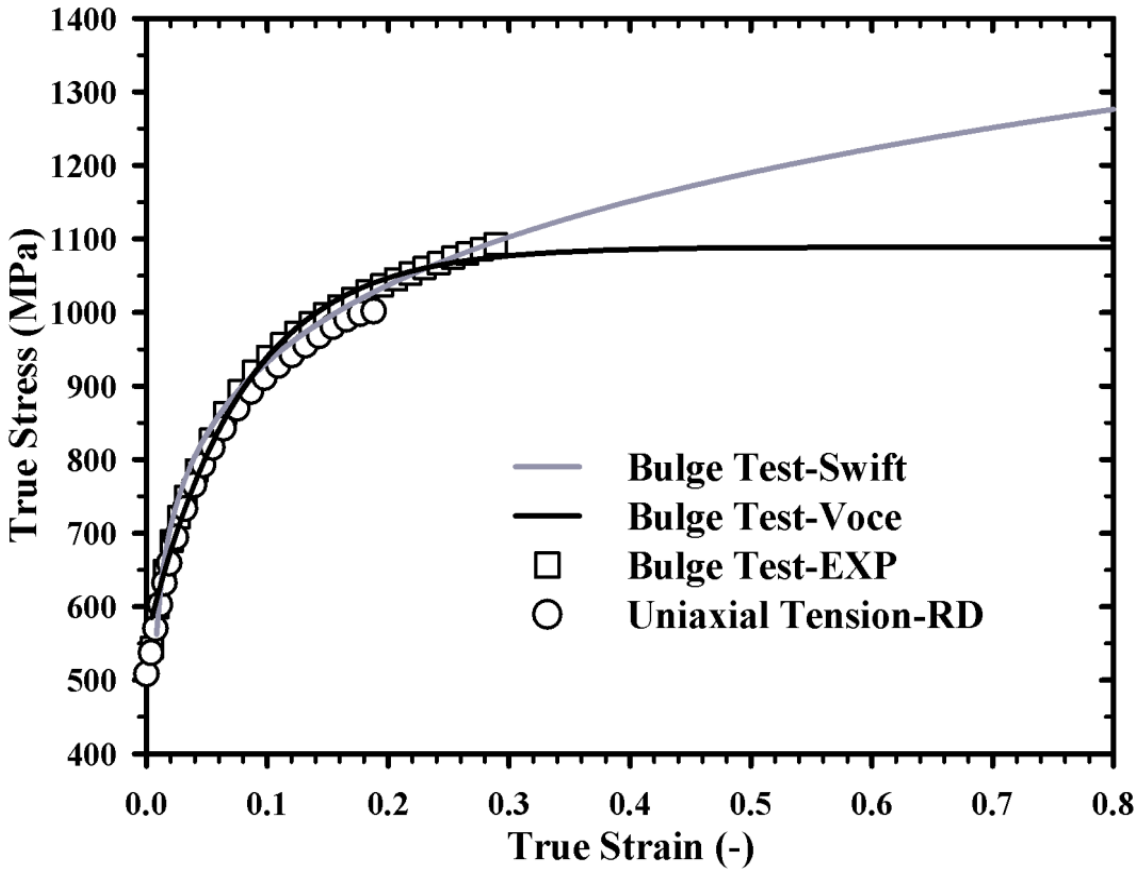

Figure 3.10 Stress-strain curves of the TRIP780 steel sheet experimentally determined by bulge test and tensile test in comparison and including extrapolation using Swift and Voce law.

An initial compressive load of 50 kN was used and the load was increased stepwise 4 kN per test until 82 kN. Three repeated tests were carried out for each load condition. After each compression increment, the diameters in the rolling direction (RD) and transverse direction (TD) were measured by three repeated time. By these measurements, the plastic true stains in the rolling and transverse directions were calculated according to the Equation 3.3.

$$\varepsilon_{RD} = \ln\left(D_{RD}/D_{RD}^{0}\right), \varepsilon_{TD} = \ln\left(D_{TD}/D_{TD}^{0}\right) \tag{3.3}$$

Where D_{RD}^{0} and D_{TD}^{0} are the initial diameters of the samples in the RD and TD, respectively. The obtained true strains in both directions were fitted with a linear function, as shown in Figure 3.13 - Figure 3.15. The r_b value defined in Equation 3.4 could be evaluated from the slope of the fitted line. Here, the averaged balanced biaxial r_b values were thus calculated to be 0.926, 0.900 and 1.022 for the DP780, TRIP780 and JAC780Y steels, respectively.

$$r_b = \frac{d\varepsilon_{TD}}{d\varepsilon_{RD}} \tag{3.4}$$

Figure 3.11 Disk compression test installed on the MTS testing machine [4]

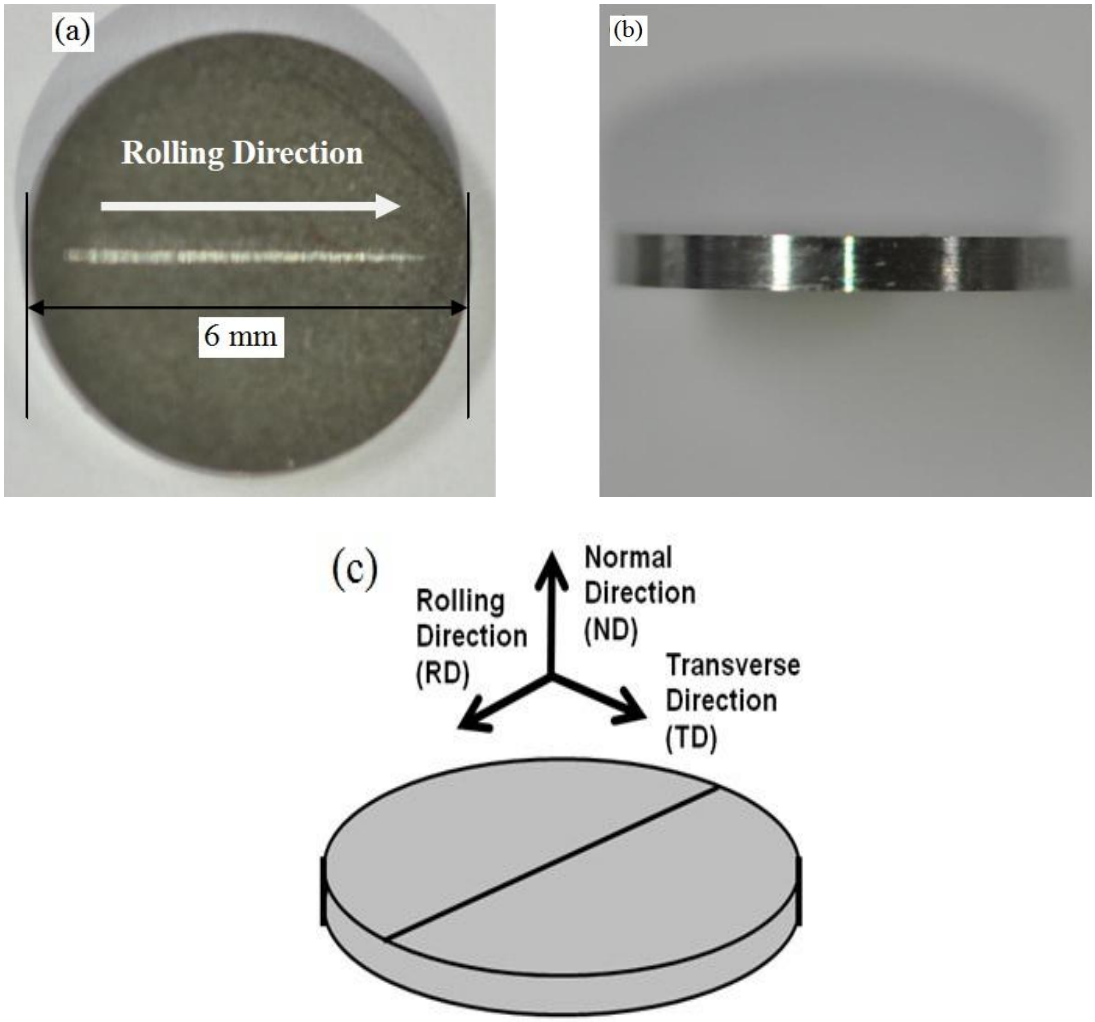

Figure 3.12 Disk Specimen (a) Front view (b) Side view (c) Schematic of direction [4]

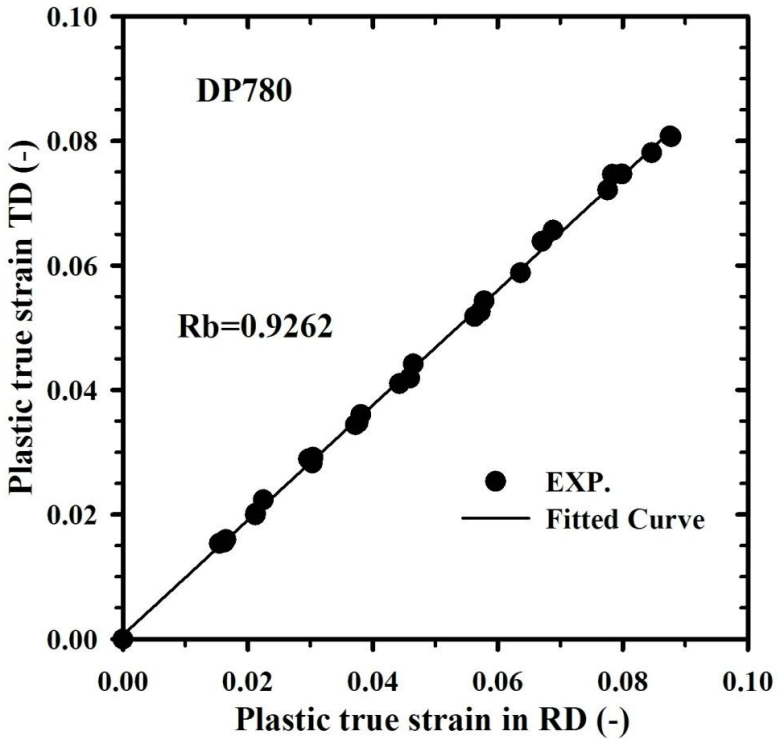

Figure 3.13 Relationship between determined plastic strains in the RD and TD of the DP780 steel

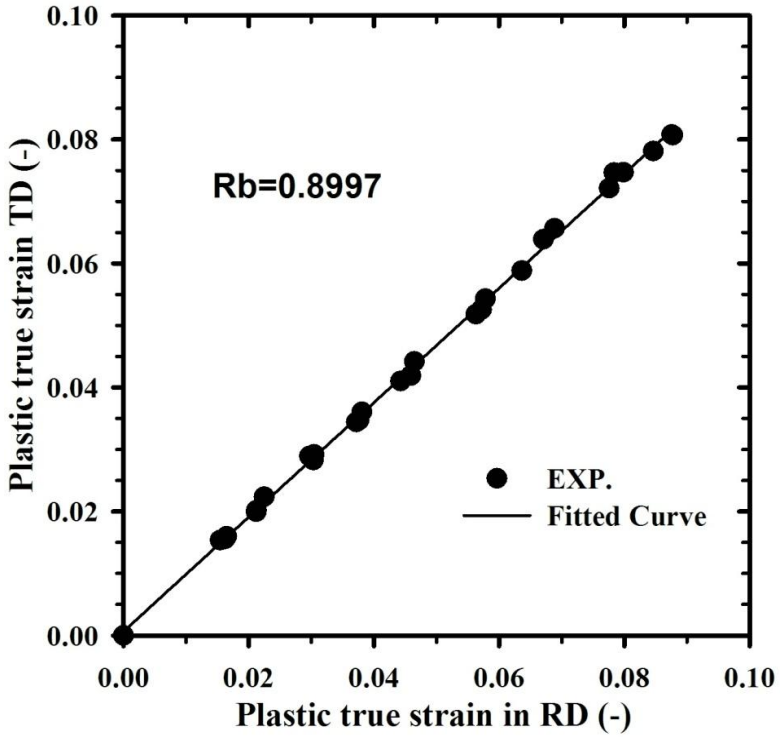

Figure 3.14 Relationship between determined plastic strains in the RD and TD of the TRIP780 steel

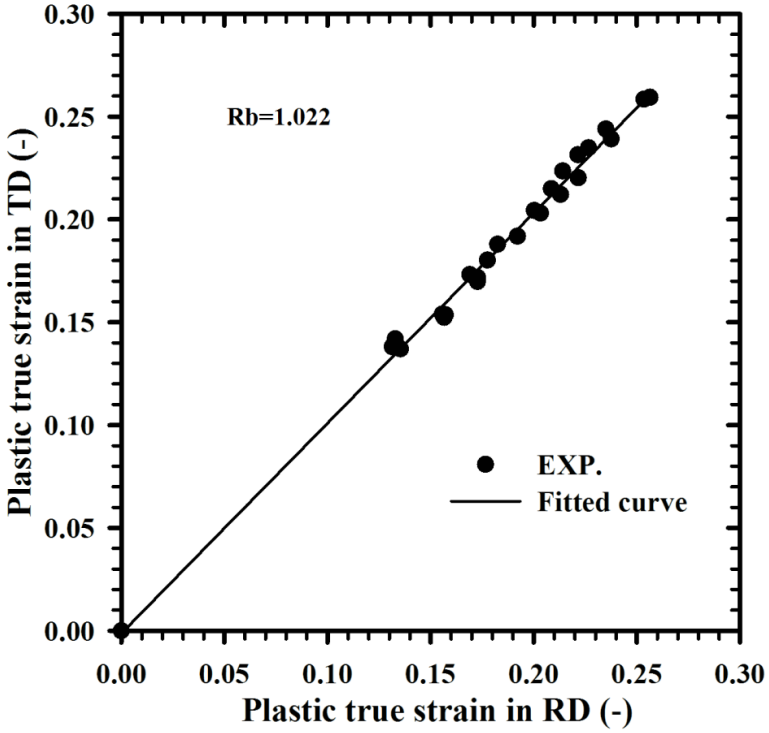

Figure 3.15 Relationship between determined plastic strains in the RD and TD of the JAC780Y780 steel.

3.2 Hardening and anisotropy characteristics

3.2.1 Anisotropic yield functions and hardening model for the TRIP780 steel

Table 3.2 showed the experimentally determined results from the uniaxial tensile tests of the investigated steel TRIP780 prepared along 0°, 45° and 90° to the rolling direction (RD). Three yield criteria, the von Mises, Hill'48 and Yld2000-2d, were applied for describing plastic behavior of the examined steel sheet. The von Mises model represented yield behavior of material as isotropic, while the Hill'48 and Yld2000-2d model took into account anisotropic plastic deformation characteristics of the material. The anisotropy coefficients for the Hill'48 criterion were calculated based on the *r*-values at 0°, 45° and 90° to the RD and the uniaxial yield stress in the RD, as presented in Table 3.7. For the Yld2000-2d criterion, required materials parameters were the uniaxial yield stresses, *r*-values at 0°, 45°, and 90° to the RD, balanced biaxial stress σ_b and balanced biaxial r_b value. Two hardening laws, the Swift and Voce model, as expressed in Equation 2.16 and Equation 2.17, respectively, were used to describe the biaxial stress-strain curve obtained from the hydraulic bulge test, as illustrated in Figure 3.10.Then, the yield stresses and yield stress ratios could be evaluated and summarized in Table 3.8 and 3.11. The yield stresses calculated by the Voce type hardening model were somewhat higher than those calculated by the Swift type hardening model. Entirely, eight experimental parameters including four yield stresses, $\sigma_0, \sigma_{45}, \sigma_{90}, \sigma_b$ and four *r*-values, r_0, r_{45}, r_{90}, r_b were used in conjunction with a system of non-linear algebraic formulations from Equation 2.9 to Equation 2.15 to determine the anisotropic coefficients α_i involved in the Yld2000-2d yield function [7]. Since the TRIP steel mainly had a microstructure consisting of ferrite, bainite, and small amount of retained austenite, the exponent of the Yld2000-2d model was set to be 6 or 7, as recommended for BCC crystal structures [7,41,59]. The calculated anisotropic coefficients were

demonstrated separately for different hardening laws and *M* values in Table 3.9 and Table 3.10 and Table 3.12 and Table 3.13. Obviously, it was found that different hardening functions and *M* value obviously led to varying yield stress and anisotropic coefficient values that consequently affected predictions of plastic deformation behavior.

Table 3.7 Determined anisotropic coefficients of the Hill'48 criterion (*r*-values based)

F	*G*	*H*	*N*
0.39115	0.53172	0.46828	1.38605

Table 3.8 Experimentally determined yield stresses and yield stress ratios according to Voce type hardening law at a plastic strain of 0.01

Test condition	Yield stress σ_i (MPa)	Yield stress ratio (σ_i/σ_0)
Uniaxial tension at 0º	607.76	1.0000
Uniaxial tension at 45º	620.08	1.0203
Uniaxial tension at 90º	635.30	1.0453
Balanced biaxial tension	662.96	1.0908

Table 3.9 Calculated anisotropic coefficients of the Yld2000-2d model with *M* = 6 and Voce hardening law

α_1	α_2	α_3	α_4	α_5	α_6	α_7	α_8
0.94866	0.98027	0.90836	0.93405	0.97071	0.78125	0.96617	1.06978

Table 3.10 Calculated anisotropic coefficients of the Yld2000-2d model with *M* = 7 and Voce hardening law.

α_1	α_2	α_3	α_4	α_5	α_6	α_7	α_8
0.97691	0.95759	0.89380	0.93514	0.96853	0.79889	0.96853	1.06527

Table 3.11 Experimentally determined yield stresses and yield stress ratios according to Swift type hardening law at a plastic strain of 0.01

Test condition	Yield stress σ_i (MPa)	Yield stress ratio (σ_i/σ_0)
Uniaxial tension at 0º	576.59	1.0000
Uniaxial tension at 45º	590.64	1.0244
Uniaxial tension at 90º	608.95	1.0561
Balanced biaxial tension	627.85	1.0889

Table 3.12 Calculated anisotropic coefficients of the Yld2000-2d model with *M* = 6 and Swift hardening law

α_1	α_2	α_3	α_4	α_5	α_6	α_7	α_8
0.96507	0.95644	0.92377	0.93106	0.96961	0.78310	0.96358	1.05803

Table 3.13 Calculated anisotropic coefficients of the Yld2000-2d model with M = 7 and Swift hardening law

α_1	α_2	α_3	α_4	α_5	α_6	α_7	α_8
0.99186	0.93496	0.90917	0.93186	0.96772	0.80098	0.96570	1.05381

3.2.2 Anisotropic yield functions and hardening model for the DP and TRIP780

Consequently, the material characterization of the anisotropic yield functions, Hill's 48 and Yld2000-2d, were calculated using the data from Table 3.4 and Table 3.5 for the DP780 and TRIP780 steels with the same calculation procedure as previous described. The anisotropy coefficients for the Hill's 48 were listed in Table 3.14 and Yld2000-2d was presented in Table 3.15 and Table 3.16 were used to describe material behavior in chapter 5.

Table 3.14 Hill's 48 anisotropic coefficients for the DP780 and TRIP780 steels

Steel	F	G	H	N
DP780	0.4639	0.5548	0.4452	1.3738
TRIP780	0.3912	0.5317	0.4683	1.3861

Table 3.15 Anisotropic coefficients of the Yld2000-2d model for the DP780 steel

α_1	α_2	α_3	α_4	α_5	α_6	α_7	α_8
0.8027	1.2190	0.7719	1.0189	1.0086	0.8991	1.0023	1.2082

Table 3.16 Anisotropic coefficients of the Yld2000-2d model for the TRIP780 steel

α_1	α_2	α_3	α_4	α_5	α_6	α_7	α_8
0.9651	0.9564	0.9238	0.9311	0.9696	0.7831	0.9636	1.0580

Additionally, stress-strain curves from uniaxial tension test (RD) for the DP780 and TRIP780 steels were fitted and extrapolated with the Swift and modified Voce hardening law as illustrated in Figure 3.17. The resulted material parameters were listed in Tables 3.17 and Table 3.18, respectively.

Table 3.17 Materials constants of the Swift hardening model

Materials	K	ε_0	n
DP780	1312.6	0.002	0.142
TRIP780	1351.0	0.007	0.169

Table 3.18 Materials constants of the modified Voce hardening model.

Materials	A	B_0	B_1	C
DP780	956.467	358.598	279.400	25.324
TRIP780	962.972	359.032	295.427	17.965

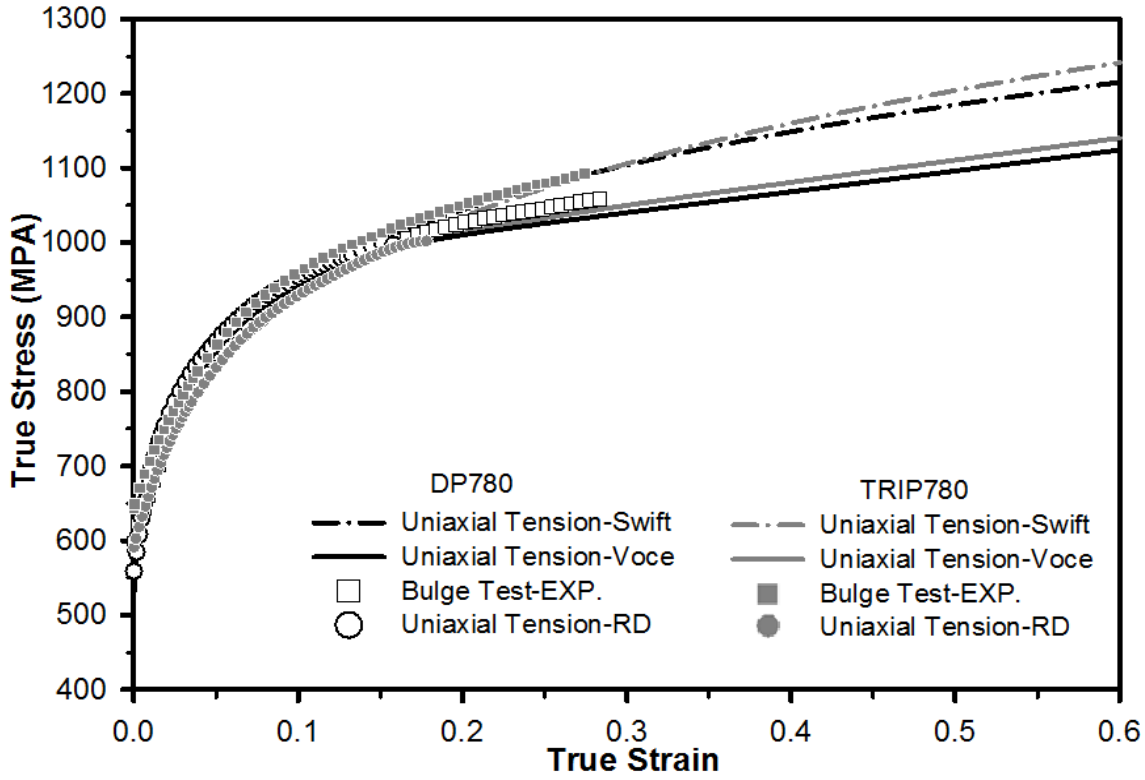

Figure 3.16 Experimental and extrapolated stress-strain curves of the DP780 and TRIP780 steels

3.2.3 Anisotropic yield functions and hardening model for the JAC780Y

Consequently, the material characterization of the anisotropic yield functions, Hill's 48 and Yld2000-2d, were calculated using the data from Tables 3.6 for the JAC780Y steel with the same calculation procedure as previous described. The anisotropy coefficients for the Hill's 48 were listed in Table 3.19 and Yld2000-2d was presented in Table 3.20

Table 3.19 Hill's 48 anisotropic coefficients for the JAC780 steel

Steel	F	G	H	N
JAC780Y	0.2379	0.3309	0.6692	1.6119

Table 3.20 Anisotropic coefficients of the Yld2000-2d model for the JAC780Y

α_1	α_2	α_3	α_4	α_5	α_6	α_7	α_8
0.79744	0.91797	0.52490	0.88530	0.91488	0.39695	0.89857	1.30129

Similarly, the JAC780Y steel was performed the mechanical tests to obtain stress-strain curves in which were fitted and extrapolated with the Swift hardening law as displayed in Figure 3.17. The resulted material parameters were listed in Tables 3.21

Table 3.21 Materials constants of the Swift hardening model.

Materials	k	ε_0	n
JAC780Y	1226.440	0.002	0.136

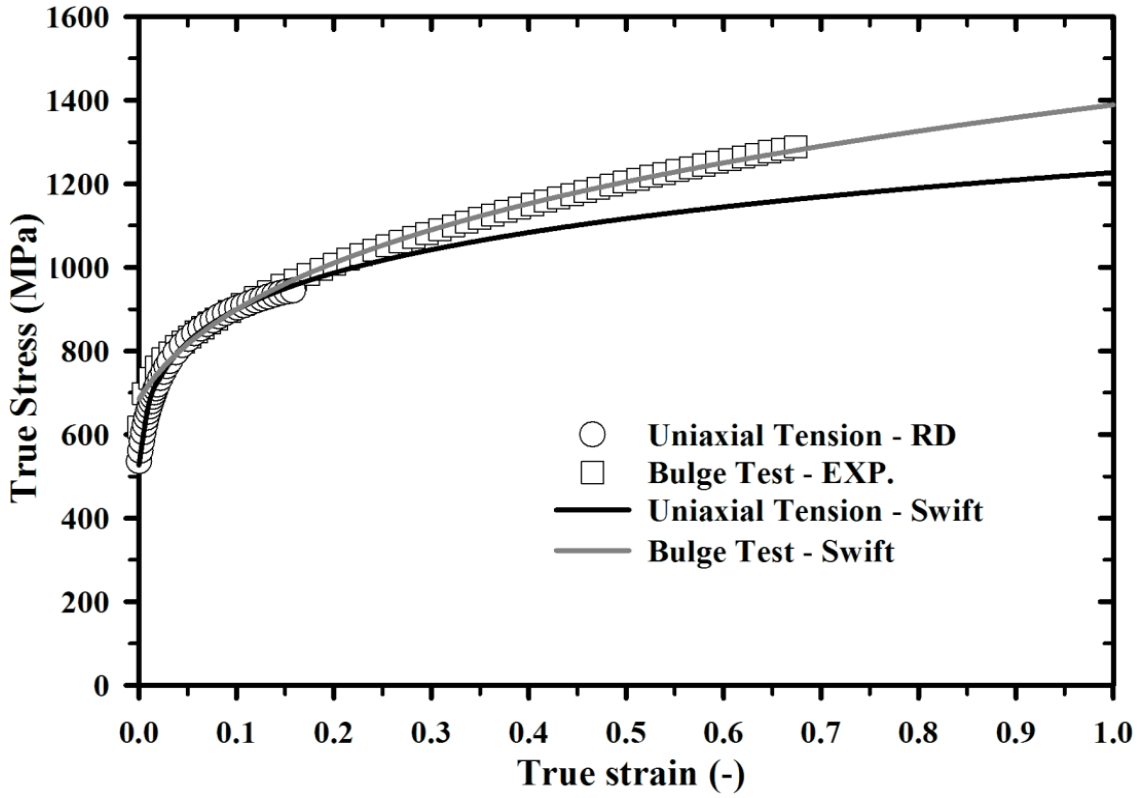

Figure 3.17 Stress-strain curves of the JAC780Y steel experimentally determined by bulge test and tensile test in comparison and including extrapolation using Swift law

3.3 Formability characterization

3.3.1 Nakazima stretch-forming test

The Forming limit Diagram (FLD) is often used as a conventional tool for formability prediction in sheet metal forming processes. The FLD is a strain based failure criterion, in which the principal in-plane strains at failure are evaluated. For experimental determination of the FLD for steels DP780,TRIP780 and JAC780Y in this work, the Nakazima stretch-forming test [60] was carried out to characterize formability limit according to a procedure suggested by international standard ISO 120004-2 [61] on a 600 kN Erichsen formability testing machine (located at MML-GIFT-POSTECH) as illustrated in Figure 3.18 and installed the Nakazima stretch-forming test as depicted in Figure 3.19. A schematic of the Nakazima test setup was shown in Figure 3.20. The used sheet metal specimens had the same length of 190 mm but different widths of 55, 85,115,125,135,165,175,190 and 195 mm were used to describe different states of stress as depicted in Figure 3.21. By means of the application these specimen geometries, a wide interval of the state of stress between uniaxial and biaxial tension stress was allowed. The initial thickness of the sheet specimens of both steel grades was 1.2 mm for DP780 and TRIP780, was 1.0 mm for JAC780Y. A pattern of square grids with a size of 2 mm was applied on the surface of the samples by electro-chemical method as demonstrated in Figure 3.22. During the test, the samples were deformed until fracture by a hemispherical punch with a diameter of 100 mm. A punch speed of 10 mm/min and a blank holder force of 300 kN were employed. Friction between sample and tooling was minimized by using tallow oil as lubricant. Consequently, the optically measured variation of the thickness reduction on Nakazima stretch-forming test was shown in Figure 3.23, the figure illustrated the thickness distribution and localized

necking areas on specimen surface at time occurring localized state. Subsequently, In Figure 3.24 depicts deformed samples after forming until failure. Additionally, the local strain analysis of the specimens was conducted by means of the optical measuring system, AutoGrid, in which local strains on the specimens were measured and computed by the software program during the entire forming test. Simultaneously, major and minor principal strains at fracture from the area in the vicinity of crack were plotted for all specimen dimensions and a forming limit curve was then constructed as presented in Figure. This forming limit curve distinguishes range of strain between safety and failure in a sheet forming process. However, some investigations showed that the FLD can move to higher or lower strain levels when the forming history or strain path in the process changes.

Figure 3.18 Erichsen formability testing machine

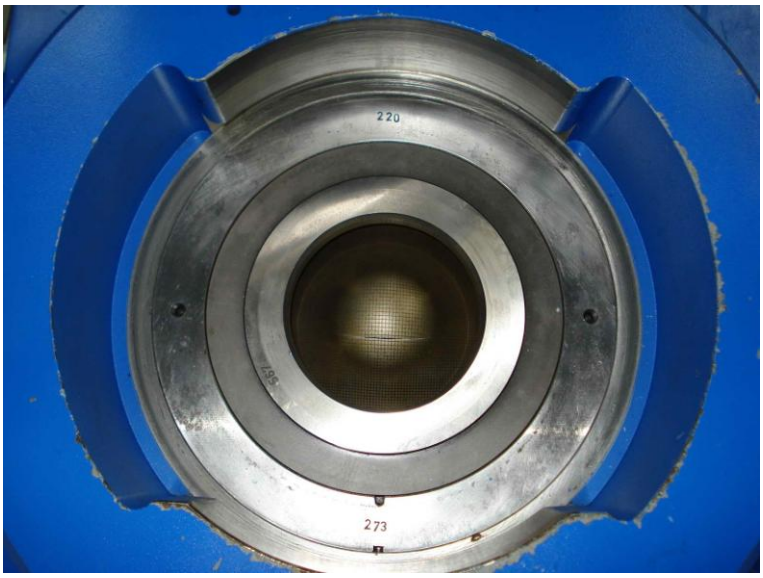

Figure 3.19 The Installed Nakazima stretch-forming test on Erichsen testing machine

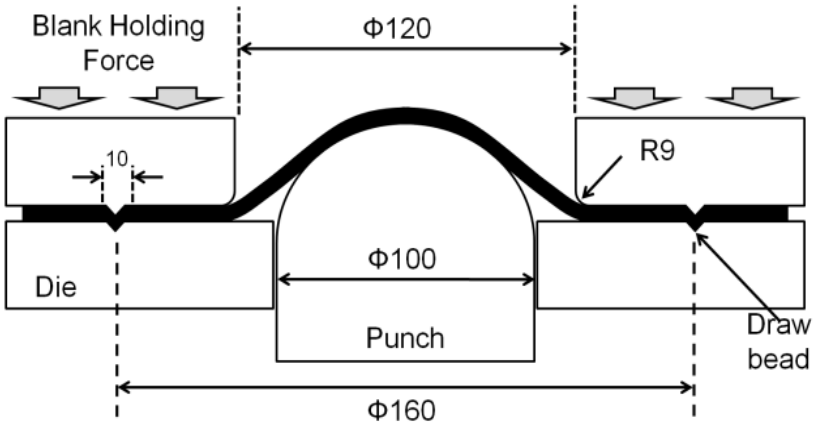

Figure 3.20 Schematic of the Nakazima test

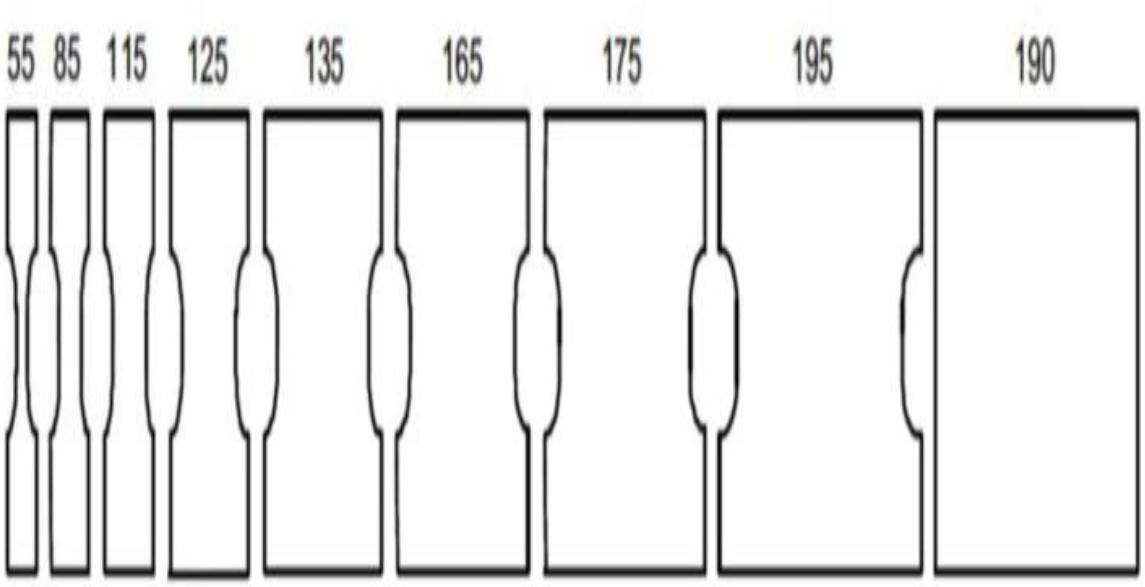

Figure 3.21 Specimen dimensions used for the Nakazima test

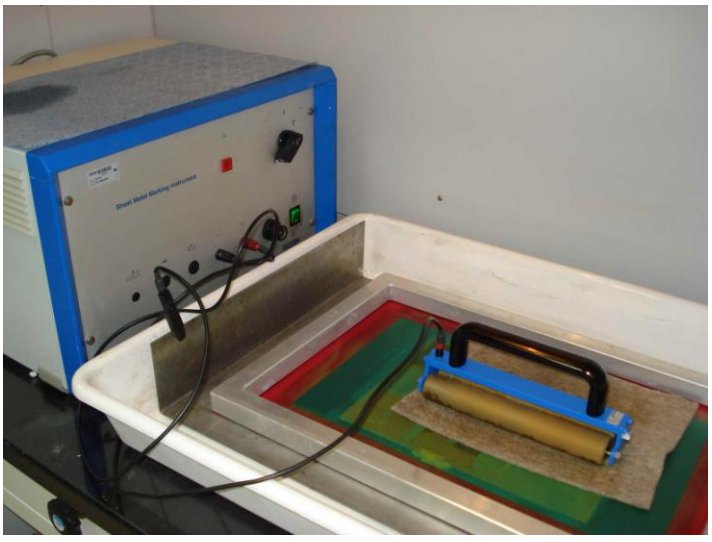

Figure 3.22 The set up of electro chemical method applied on the sample surface

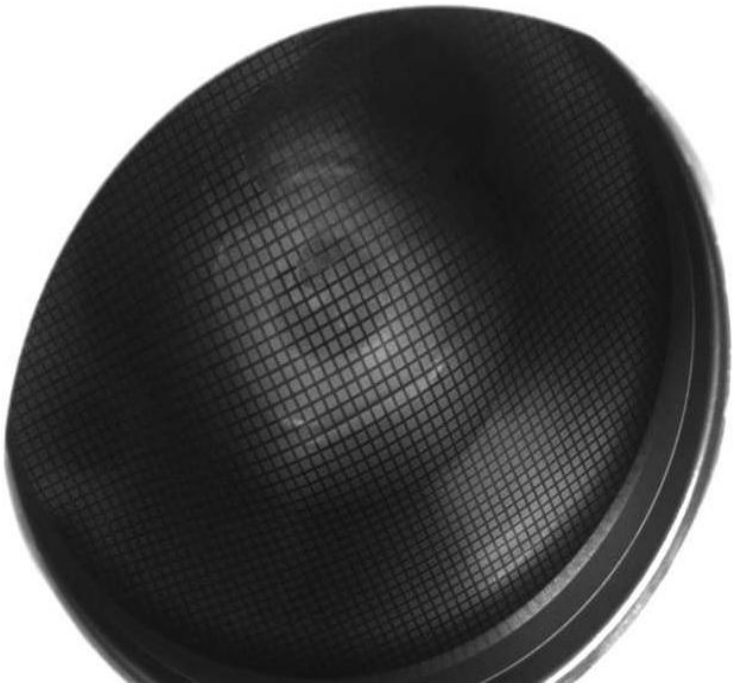

Figure 3.23 Thickness distribution and localized necking area on the deformed specimen at localized state during test

Figure 3.24 Deformed specimens after failure in the Nakazima test.

3.3.2 Hole expansion test

The hole expansion test provided a special procedure for evaluating stretch-flangeability of material, in which radial compressive and tangential tensile stresses were allowed simultaneously in the vicinity of the hole area [46]. Critical state of stress occurred in the hole expansion test located on the left hand side of the strain based diagram between uniaxial and plane strain tension. Hole expansion tests with flat bottom punch were performed on Erichsen formability testing machine at MML-GIFT-POSTECH. Specimens with a wire cutting hole in the centre were prepared for the investigated steel sheets, DP780 and TRIP780. During the test, specimen with a central hole was firstly clamped between the blank holder and upper die. Movement of the outer sample periphery was prevented by means of a high constant blank holder force of 60 kN. Then, punch force was applied with a velocity of 20 mm/min. Once, the punch force suddenly dropped due to an appearance of crack, the test was terminated. Schematic view of the experiment was depicted in Figure 3.25 and also the hole expansion test on Erichsen formability test machine was installed as demonstrate in Figure 3.26. Experimentally, the hole expansion tests were performed until failure state the machine stop, the deformed hole expansion specimen before crack occurring state shown in Figure 3.27(a) and failure deformed hole specimen is presented in Figure 3.27(b), respectively. The initial hole diameter d_0 was 12 mm. After the test, diameter of the enlarged hole, d, was measured to calculate the hole expansion ratio (initial diameter proportional to end diameter), which is generally utilized to characterize the limitation of formability of blanks in hole flanging process. Punch load and stroke, thickness strain distribution on the specimen surface along the hole circumference and along the specimen diameter in the rolling and transverse direction were only determined for steel TRIP780 comparison with the FE simulation of these tests with the same boundary conditions, in which will be described in the next chapter 4. Consequently, the force-displacement curves from the experiments were determined and compared with the FE simulations of the hole expansion test with the same boundary conditions for both DP780 and TRIP780 steels, in order to verify the simulation results and to identify the point of time when failure took place during the experiments, will be discussed in the chapter 5 in details.

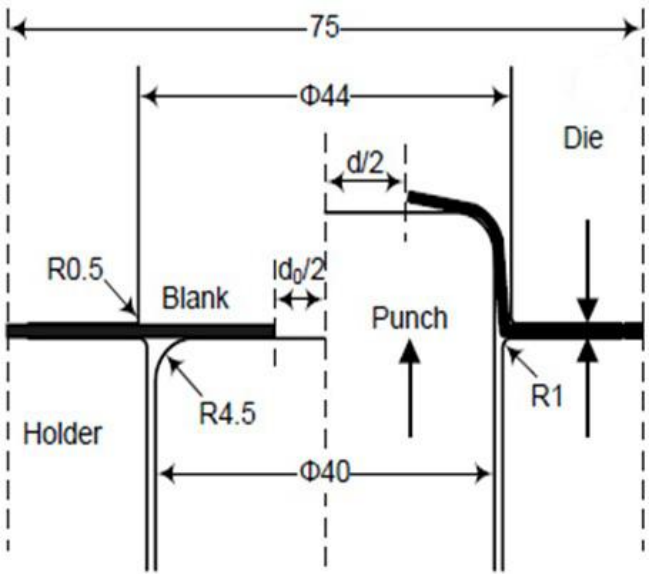

Figure 3.25 Schematic of hole expansion test using flat bottom punch (dimension in mm)

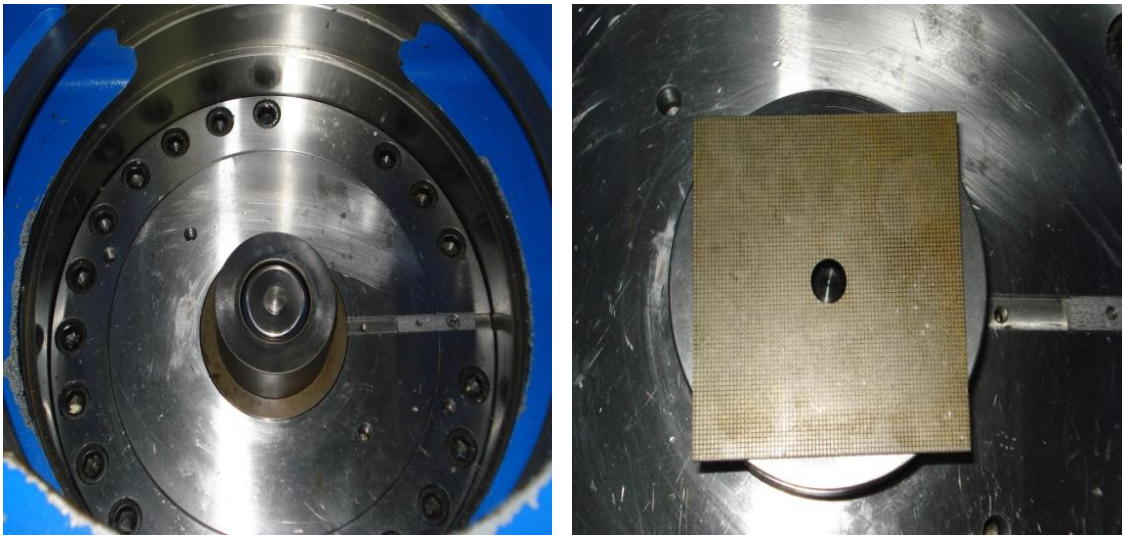

Figure 3.26 Hole expansion test installed on Erichsen formability testing machine

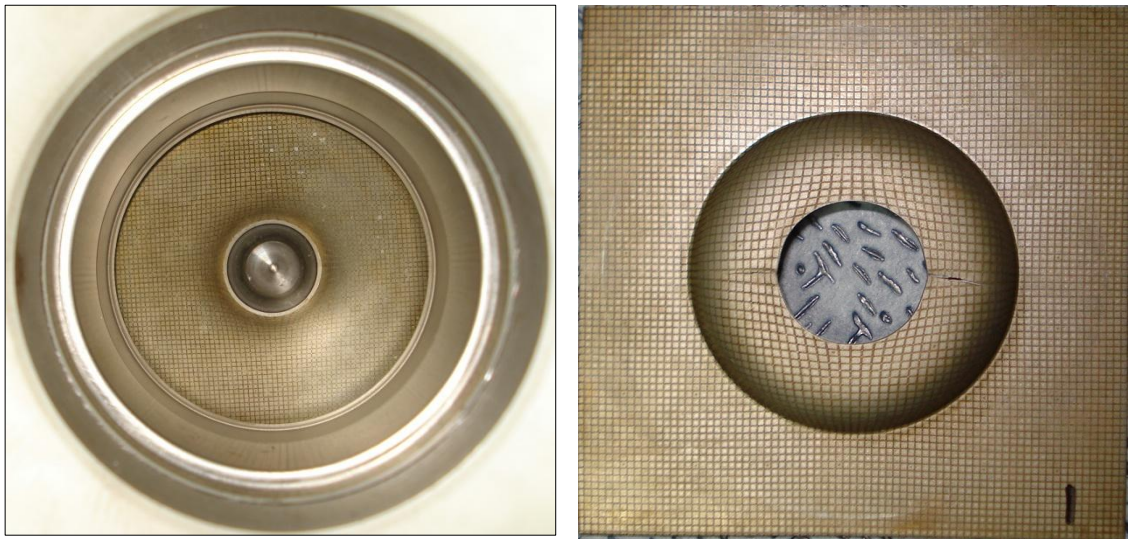

(a) (b)

Figure 3.27 Deformed hole expansion specimens at (a) before crack and (b) crack state

3.4. Determination of damage criteria using hybrid method

To determine the damage criteria for representing ductile crack initiation locus (DCIL) and plastic instability state of the investigated DP steel, a hybrid method between experiments and numerical FE simulations was employed.

3.4.1 Hybrid approach

Firstly, a series of tensile tests using samples with various geometries, which covered a widely broad range of stress states between 0 and 0.667, was carried out. During the tensile test, force and displacement curves were obtained until fracture. Simultaneously, the direct current potential drop (DCPD) method was conducted on the sheet samples for identifying state of crack initiation within the critical areas. By the DCPD method, elongation, force and time, at which crack initiated were determined. In addition, the moment, when the maximum force was reached in the tensile tests, was considered as

the onset of plastic instability. The corresponding FE simulations of the tensile tests of various specimens were performed, in which different yield criteria were defined. The force–displacement curves obtained from the experiments and simulations until failure were compared. By this manner, calculated stress triaxialities and equivalent plastic strains in the identified fractured area at the critical point of time or displacement were gathered, which represent the onset of both crack initiation and plastic instability. The obtained values were taken to construct a failure limit curve or so–called damage curve as a relation of effective plastic strain and stress triaxiality.

3.4.2 Identification of crack initiation

Basically, visual method or digital image correlation (DIC) is used to detect macro–crack formation in sheet metals under deformation, as shown in Hancock [51], Bao and Wierzbicki (50) and Dunand and Mohr [62]. The cracks with the size of about 0.1 mm could be recognized. Alternatively, developed in 1950, a more conservative method, the direct current potential drop (DCPD) method has been used to identify onset of stable crack initiation in those fracture mechanics tests. The test set up of this DCPD method could be applied to tensile notched samples for determination of failure in high strength steels (63). The similar approach was successfully utilized by Lian et al. (64), Uthaisangsuk (1) and Muenstermann (65) for advanced high strength steels. This method can be applied by using both alternating and direct currents. Alternating currents provide a higher resolution, but require a more complex test setup. For high frequency current, it induces the skin effect, which reduces its ability to detect crack initiation on the surfaces. On the other hand, the DCPD method requires a simple test setup and considers the complete cross section of the specimen, but is susceptible to disturbance from thermoelectric effects (63).

A schematic setup of the experiments is demonstrated in Fig. 6. A direct current is supplied to conduct the current flow through the gauge section of the samples. The current of 1.25 A was selected according to the material and dimension of the sample in order to obtain the constant electric current flow on the samples and also to avoid critical heating of the samples. In addition, the voltage potential in between the notched area of the samples was measured using a voltmeter (64) as shown in Figure 3.29. During the tensile tests, the constant direct current was conducted through the samples and the potential difference in the critical area was gathered. When void nucleation and growth occurred in a sample, the total cross sectional area of the sample became smaller. Due to the appearance of severe discontinuity in the material induced by coalescence of voids and resulting formation of microcrack, a sudden increase of the electric potential was then observed. At this instance, it was just the microcrack has initiated and the corresponding force and displacement were identified as the critical load and deformation, respectively.

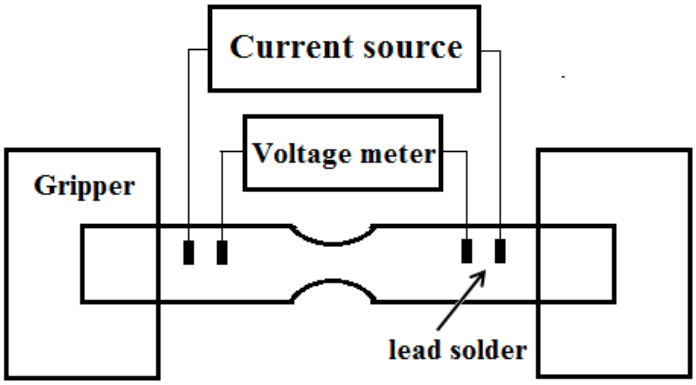

Figure 3.28 Typical setup of the DCPD method for determining crack initiation during tensile test

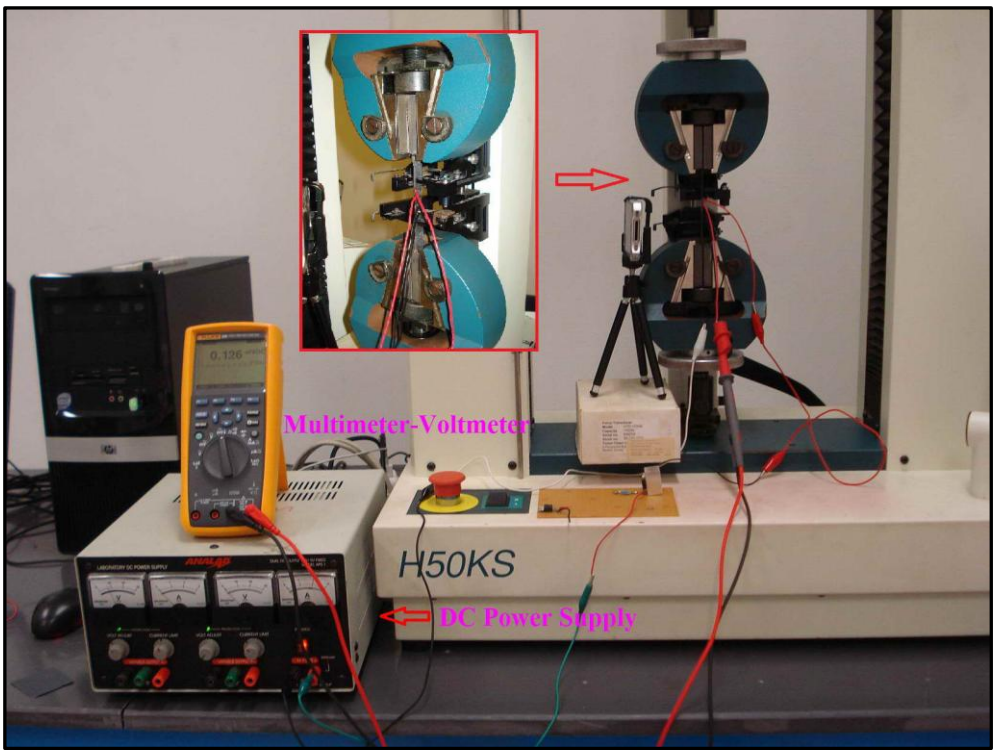

Figure 3.29 Experimental setup for determination of damage curve

3.4.3 Tensile tests of notched specimens

3.4.3.1 Low stress triaxiality range (0 – 0.4)

Three different sample geometries were used, namely, pure shear (PS), combine loading (CL) and uniaxial (Uni) sample, as depicted in Fig. 7. In the case of the pure shear sample, only shear stress occurred in the middle area during the test, but the hydrostatic stress or mean stress σ_m was zero or very small in comparison to the effective stress in the same area. This condition led to the stress triaxiality value of zero or nearly zero. For the combined loading sample, the pure shear sample was slightly modified to emulate a stress state of combined shear and tensile loading, as

demonstrated in [63] and (66). A stress triaxiality value somewhat higher than that of the pure shear sample was provided. The uniaxial sample resembled a simple dog bone tensile sample, by which a stress triaxiality of about 0.33 was established.

3.4.3.2 Medium stress triaxiality range (0.4 – 0.577)

Various notch types were defined for the tensile sample to obtain a stress triaxiality range between 0.4 and 0.577. A total of eight different notched sample geometries were used in the tests. For example, the tensile samples with radius–, C–, U–, V–notch shapes are illustrated in Fig. 8. Additionally, other two sample types, namely, the sample with central hole (H) and elliptical hole (El) were established. The central hole (H) sample contained an inner hole with a radius of 3 mm in the middle, as seen in Fig. 9a. The elliptical hole (El) sample had an elliptical cutout at the center with a constant minor radius of 2 mm. Two varied major radii of 3.5 and 7 mm, as illustrated in Fig. 9b, were used.

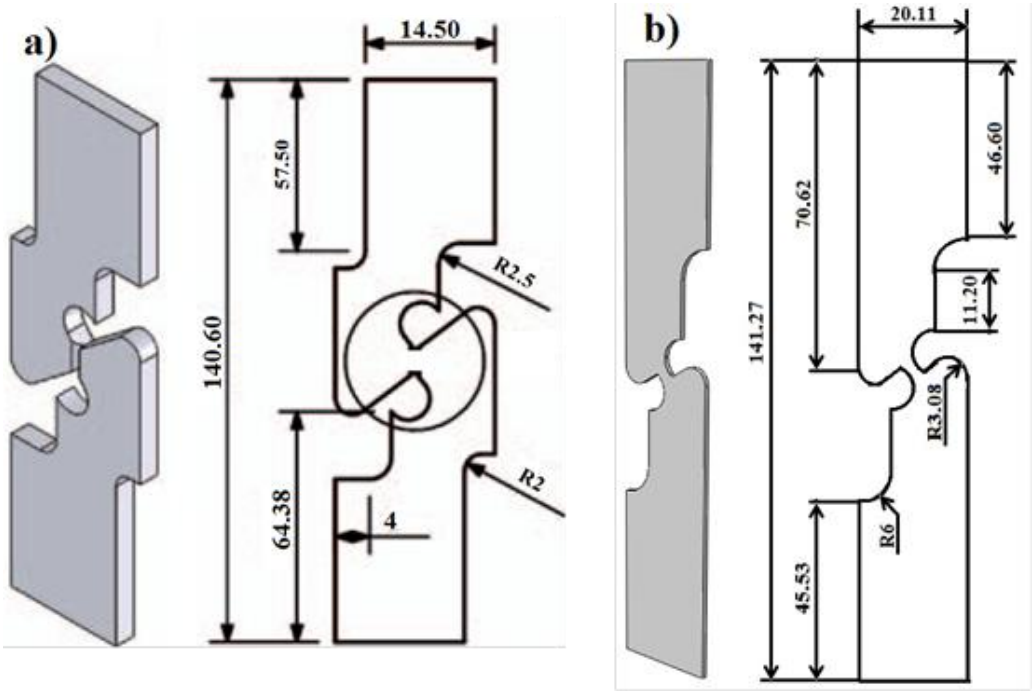

Figure 3.30 (a) Pure shear sample and (b) combined loading sample [64]

3.4.3.3 High stress triaxiality range (0.577 – 0.667)

The plane strain samples, as shown in Fig. 10, were used to generate this stress triaxiality range. All samples had the width of 50 mm and the length of 130 mm. In the samples, four different radii of grooves, 12.5, 7.5, 4 and 1.5 mm were manufactured. Note that the highest stress triaxiality value, in this work, was obtained by the hydraulic bulge test, more detail was given in 3.2.

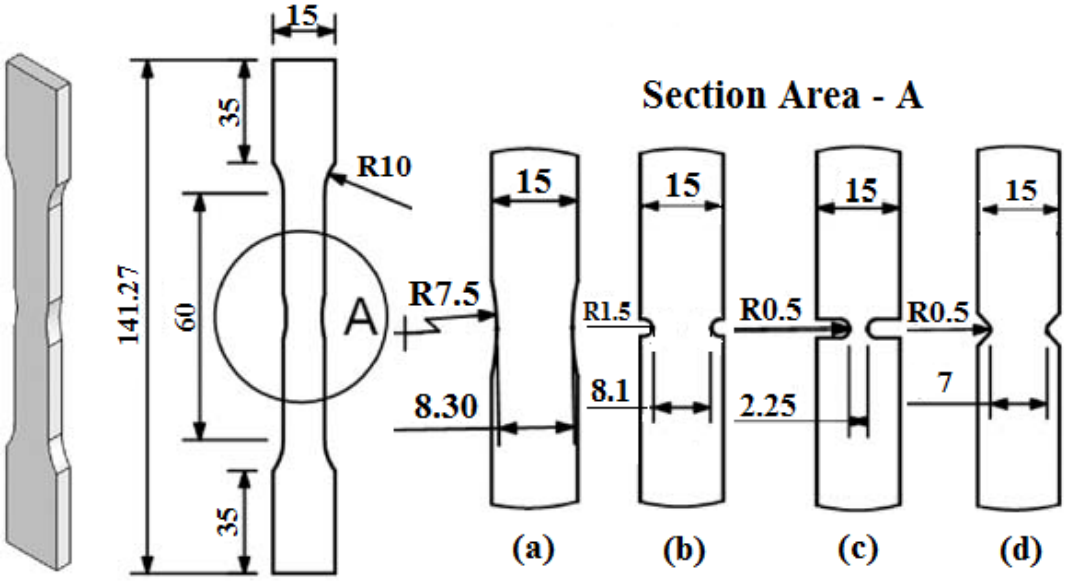

Figure 3.31 Tensile samples with (a) radius–, (b) C–, (c) U– and (d) V–notch shape[64]

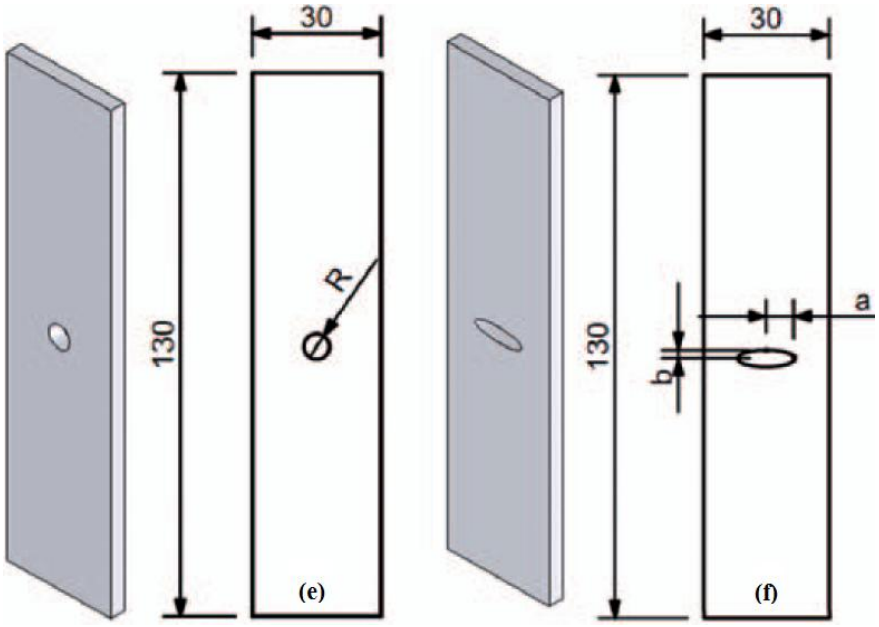

Figure 3.32 Tensile samples with (a) central hole (H) and (b) elliptical hole (El) [64]

.

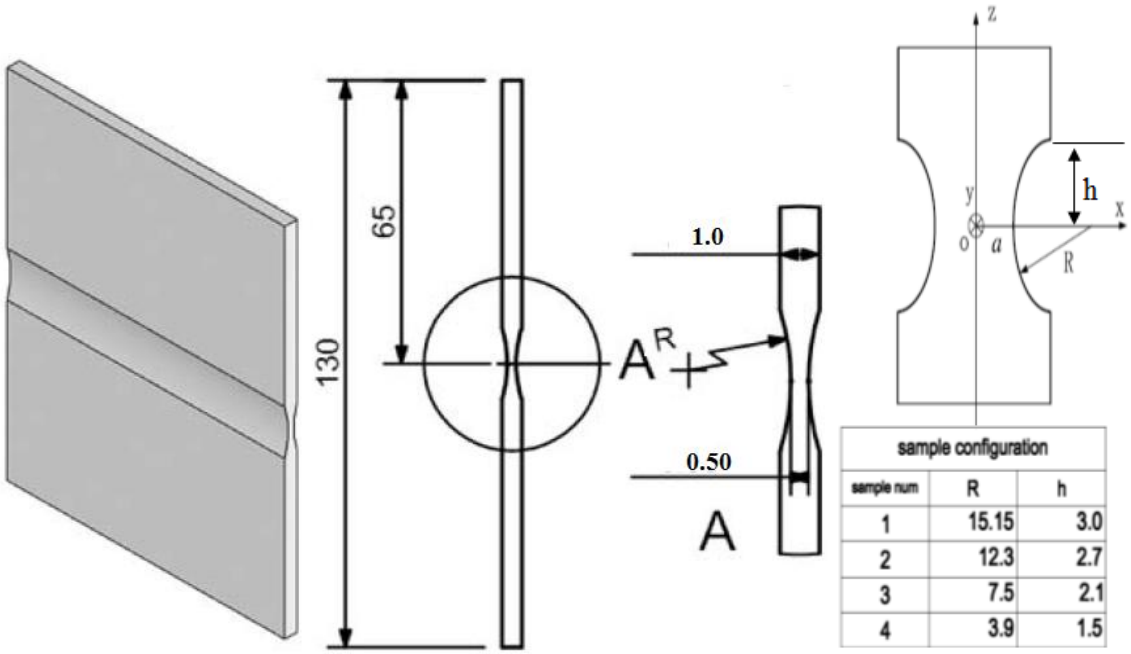

sample configuration		
sample num	R	h
1	15.15	3.0
2	12.3	2.7
3	7.5	2.1
4	3.9	1.5

Figure 3.33 Plane strain samples with transverse notches of different radii [64]

The samples with the mentioned geometries of the AHS steel grade JAC780Y with thickness of 1 mm were prepared such that the loading direction of the specimen was orientated along the rolling direction. Tensile tests of these various samples were performed on a universal testing machine. To achieve a quasi–static condition, a low crosshead speed was applied with a strain rate of 0.001 s^{-1}.The damage criteria of the investigated DP steel were neglected the effect of strain rate. Fifteen different geometries of the tensile samples were totally tested. Simultaneously, the DCPD method, as described in details in 3.4.2, was applied during all the tensile tests. Figure 6.1(a) illustrates the force–displacement curve and the potential difference curve determined from the tensile test of the U–notch sample with the DCPD method. The crack initiation point was identified by the sudden change in slope of the potential curve, and the critical load was afterwards determined.